

High Efficient Removal of Methylene Blue Using Microcrystalline Cellulose/Polyvinyl Alcohol/Expanded Graphite 3D Porous Foam as a “Green” Adsorbent

Xiaodong Tan^{1*}, Qingyan Peng¹, Tereza Subrova¹, Jana Saskova¹, Jakub Wiener¹, Mohanapriya Venkataraman¹, Jiri Militky¹, Wei Xiong², Arunjuna Raj Mahendran³, Herfried Lammer³

¹Department of Material and Textile Engineering, Technical University of Liberec, 461 17 Liberec, Czech Republic; ²Hubei Key Laboratory of Biomass Fiber and Eco-dyeing and Finishing, College of Chemistry and Chemical Engineering, Wuhan Textile University, Wuhan 430073, China; ³Wood K Plus-Competence Center for Wood Composites and Wood Chemistry, Altenberger Strasse 69, A-4040 Linz, Austria

ABSTRACT

The cellulose/Polyvinyl Alcohol (PVA)/Expanded Graphite (EG) 3D porous foam, which has wide application prospects in cost-effective dye removal, was prepared by physical crosslinking and foaming technology. The prepared foam material has an obvious 3D network and porous structure, exhibiting excellent removal efficiency for Methylene Blue (MB) in an aqueous solution. The largest MB adsorption capacity of the foam is 110.81 mg/g. The adsorption process follows the pseudo-2nd order kinetics and the Freundlich isotherm model, indicating that the adsorption process is controlled by active surface sites and the physical adsorption process. Thermodynamic studies have shown that the adsorption process is a spontaneous and exothermic reaction. After five cycles of adsorption experiments, the composite material still exhibited a more than 70% dye removal rate. The results show that cellulose/PVA/EG 3D porous foam is effective, promising, and recyclable adsorbent, which can be used to remove MB from aqueous solutions.

Keywords: Long-COVID; PASC; IL-8, IFN γ ; Immune exhaustion; SARS-CoV-2

INTRODUCTION

Dyes are widely used in the dyeing process of textiles, papermaking, pharmaceuticals, food, and other fields [1,2]. A large amount of the wastewater containing organics, which are often toxic, stable in aqueous solution, and difficult for natural degradation, are inevitably produced during the process of dyeing [3,4]. Methylene Blue (MB) is a cationic dye widely used for testing of waste water treatment. At the same time, MB has a huge negative impact on the human body, such as meningitis, neuronal cell apoptosis, nausea, and vomiting [5]. Many methods have already been applied in solving wastewater, such as membrane filtration, flocculation, co-precipitation, chemical redox, and biological treatment [6-9]. However, these methods have some restricting factors in

their application, such as high cost, unfavorable recycling, and secondary pollution.

Adsorption is a common method to sequester organic dyes from wastewater [10]. Compared with other methods, the adsorption shows low cost, high efficiency, easy recovery, and high selectivity [11]. Some traditional adsorbents have been widely discussed. Mahdi Hasanzadeh developed an activated carbon/metal-organic framework composite material to obtain extremely high adsorption capacity in the removal of anionic dyes, and the adsorption process performs the Langmuir model, which indicates chemical adsorption [12]. Lamia Dali Youcef studied the performance of a zeolite in adsorbing cationic dyes. Studies have shown that an excellent dye removal rate can be obtained at

Correspondence to: Xiaodong Tan, Department of Material and Textile Engineering, Technical University of Liberec, 461 17 Liberec, Czech Republic, E-mail: xiaodong.tan@tul.cz

Received: 22-Sep-2022, Manuscript No. JTC-22-19327; **Editor assigned:** 26-Sep-2022, PreQC No. JTC-22-19327 (PQ); **Reviewed:** 10-Oct-2022, QC No. JTC-22-19327; **Revised:** 17-Oct-2022, Manuscript No. JTC-22-19327 (R); **Published:** 24-Oct-2022, DOI: 10.37532/2157-7544.22.13.308.

Citation: Tan X, Peng Q, Subrova T, Saskov J, Wiener J, Venkataraman M, et al (2022) High Efficient Removal of Methylene Blue Using Microcrystalline Cellulose/Polyvinyl Alcohol/Expanded Graphite 3D Porous Foam as a “Green” Adsorbent. J Thermodyn Catal. 13:308.

Copyright: © 2022 Tan X, et al. This is an open-access article distributed under the terms of the Creative Commons Attribution License, which permits unrestricted use, distribution, and reproduction in any medium, provided the original author and source are credited.

a lower dye concentration [13]. Zhihui Huang studied modified bentonite to adsorb Rhodamine B and Acid Red 1. It was found that the maximum adsorption capacity of Rhodamine B and Acid Red 1 were 173.5 mg/g and 157.4 mg/g, respectively [14]. Although these traditional adsorbents are popular, they have poor regeneration ability and are toxic to many organisms. Meanwhile, these adsorbents, based on chemical adsorption during the adsorption process, are hardly reused [15]. Based on the requirements of environment-friendly adsorption, biosorbents have received extensive attention. Among them, cellulose and Polyvinyl Alcohol (PVA) are widely used as biosorbents due to outstanding characteristics such as low cost, solubility, good mechanical strength, stability, biocompatibility, and non-toxicity [16]. Expanded Graphite (EG) is a common carbon material. Compared with graphene, carbon nanotube and graphene oxide have many advantages, such as huge porosity, excellent chemical properties, thermal stability and good mechanical stability, which have significant superiority in adsorption [17,18].

As porous materials have been developed rapidly in recent decades, related research is focused on aerogels and hydrogels. 3D network materials with open porous and microporous structures show great potential in wastewater adsorption [19]. Sheng Tang developed an amphiphilic graphene aerogel for the adsorption of dyes and found the best effect on the adsorption of malachite green [20]. Shu Wang prepared a silk fibroin-modified graphene oxide-based aerogel, which showed excellent adsorption capacity in MB [21]. However, some problems of studied porous materials include expensive raw materials, costly manufacturing, and complicated drying process [22,23].

Foam materials also have an open porous structure, convenient preparation process, and extremely low production cost for wider use [24]. The trimethylammonium grafted cellulose foam prepared by Chuting Feng can selectively adsorb anionic dyes and obtain better adsorption performance [25]. Hong Ma developed flexible cellulose foam to obtain high adsorption capacity (116 mg/g) [26].

In this work, we prepared the cellulose/PVA/EG 3D porous foam by developing a simple and feasible strategy for the removal of methylene blue. After simple foaming and solidification, the prepared foam has a stable 3D and open porous structure, which can efficiently and cyclically remove methylene blue and has broad application in dye wastewater treatment.

METHODOLOGY

Materials

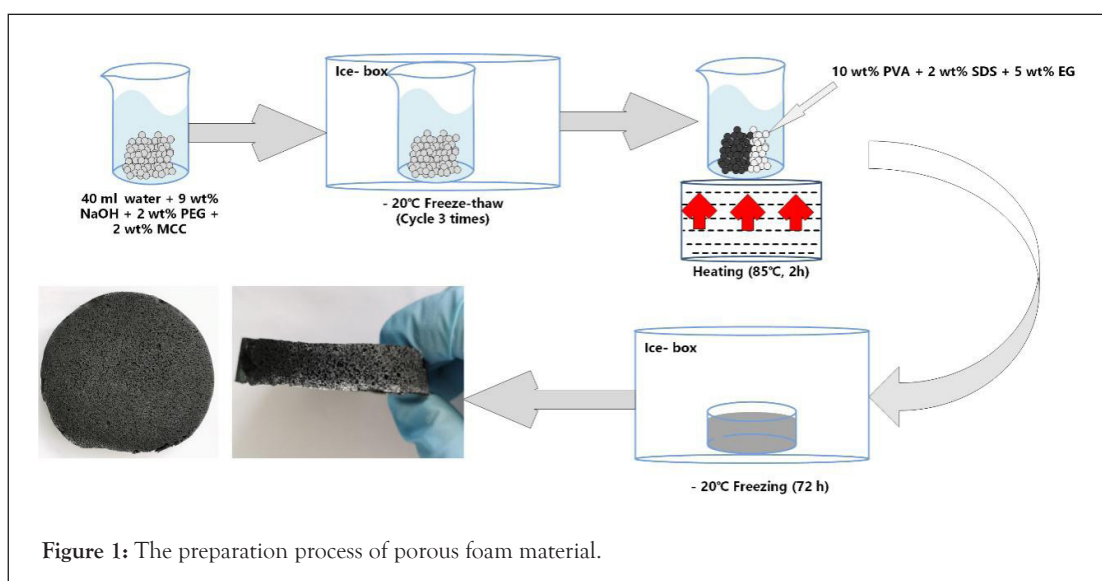
Microcrystalline Cellulose (MCC, 98%, 20 μm), PVA (molecular weight 72000), Sodium Dodecyl Sulfate (SDS, 99%), Sodium Hydroxide (NaOH), Polyethylene Glycol 4000 (PEG), MB, and Ethanol were supplied by Sigma Aldrich (ST. Louis, USA). EG was provided by the Technical University of Liberec. All the solutions used distilled water with 18 M Ω cm electrical resistivity.

Preparation of cellulose solution in PEG + NaOH system

The procedure of cellulose solution was carried out according to the method reported by Yan and Cernencu [27,28]. At first, 2 wt% PEG and 9 wt% NaOH were dissolved in 40 ml of distilled water. Then, 2 wt% MCC was added to this solution, continuously stirring for 3 hours. Finally, the suspension was frozen at -20°C for 12 hours and then thawed at room temperature. This step was repeated three times.

Preparation of 3D porous foam material

At first, 10 wt% PVA and 5 wt% EG were added into the suspension with stirring at 600 rpm and 85°C for 3 hours. Then 2 wt% SDS was added with stirring for 30 minutes to emulsify and foam the suspension. At last, the suspension was frozen for solidification at -20°C for 72 hours. After thawing, the porous foam material was obtained (Figure 1). Herein, samples were named according to the composition of the added chemicals, such as PVA+SDS (PS), MCC+PVA (CP), MCC+PVA+SDS (CPS), and MCC+PVA+SDS+EG (CPSG).



Morphology test of different composites

The surface morphology of porous foam material was observed by Scanning Electron Microscope (SEM) (VEGA TESCAN Inc., USA) [29].

Adsorption experiment of MB

For the adsorption experiment, MB was chosen as a model dye to check the adsorption property of porous foam materials. In short, different concentration solutions of MB were prepared by dilution for construction of the calibration curve (Figure 2). Then, we put 0.06 g sample into 30 ml different concentration solution of MB (25 mg/L, 50 mg/L, 100 mg/L, 150 mg/L, 200 mg/L, 250 mg/L). UV-spectrophotometer (7415, Cole-Parmer Ltd.) was utilized to determine the concentration of residual MB dye in the solution after adsorption at 665 nm wavelength. The dye removal efficiency and adsorption capacity were calculated according to equation 1 and 2 [30].

$$Removal\ percentage(R\%) = \frac{c_o - c_t}{c_o} \times 100\% \dots\dots\dots(1)$$

$$Adsorption\ capacity(q_t) = \frac{(c_o - c_t) \times v}{m} \times 100\% \dots\dots\dots(2)$$

Where c_o , c_t (mg/L) are the concentrations of MB at zero time and time t, respectively. v is the MB solution volume (L) and m (g) is the mass of the sample.

Recycling test

The sample containing adsorbed MB was placed into absolute ethanol solution for 72 hours at room temperature. Then, the adsorption experiment was repeated after most MB was desorbed from samples.

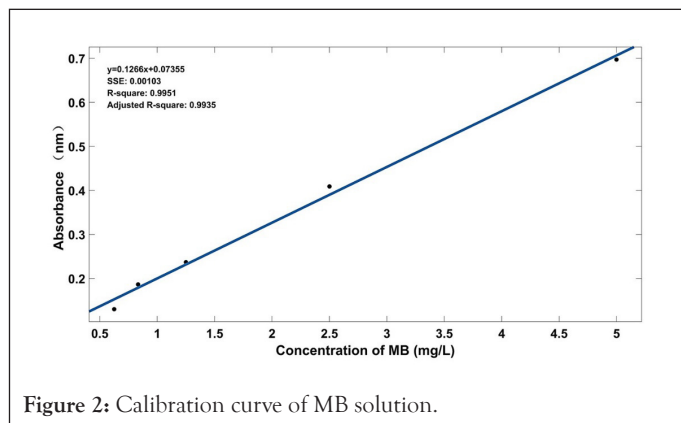


Figure 2: Calibration curve of MB solution.

RESULTS AND DISCUSSION

Surface morphology of different structures

As we can see from Figure 3, it can be clearly observed that CPS and CPSG have a 3D porous structure. In contrast, PS only forms a 2D film, and CP forms a 3D structure without porous structure. At first, as a water-soluble, soft, and long-chain polymer, PVA has widely been applied in the preparation of permeable membrane, aerogel, and hydrogel due to its excellent film-forming and excellent chemical properties [31]. However, even if we added any foaming agent in this research, there was still no porous structure.

This may be because we utilized freezing instead of freeze-drying in this experiment. So, in the subsequent thaw process, its 3D structure collapsed. In addition, bubbles generated by the foaming agent could not form porous structure in the final solidification due to the collapse of the overall structure.

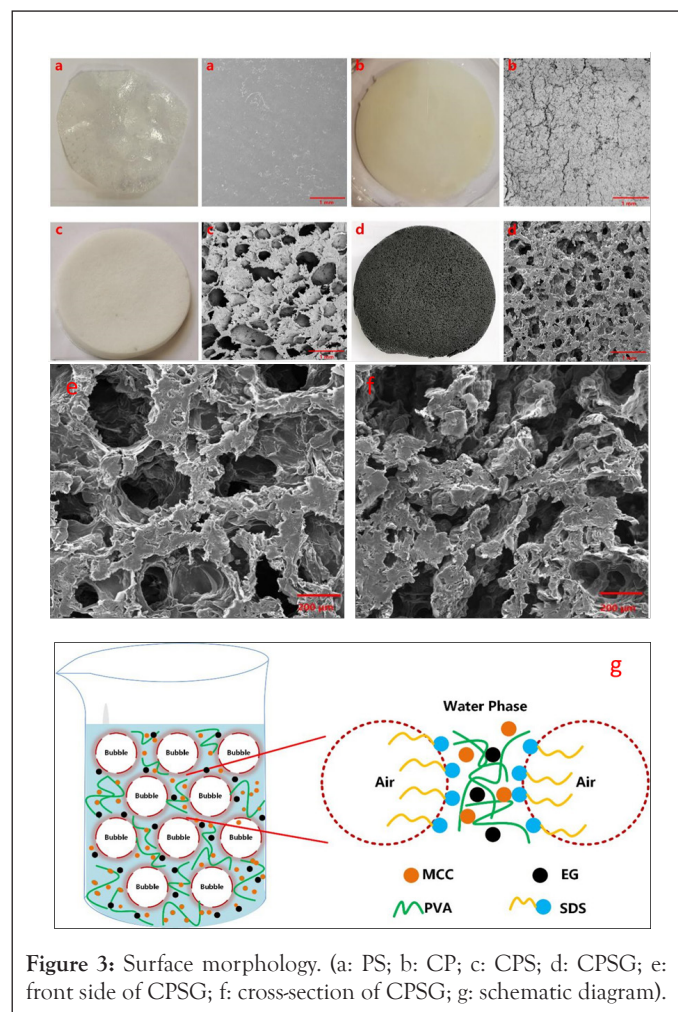


Figure 3: Surface morphology. (a: PS; b: CP; c: CPS; d: CPSG; e: front side of CPSG; f: cross-section of CPSG; g: schematic diagram).

In contrast to CP, CPS and CPSG formed a good 3D structure. The main reason is the addition of cellulose. It is well-known that cellulose consists of a well-organized crystallinity region that contributes to the strength, high stiffness, and amorphous region, which makes fiber more flexible [32,33]. Cellulose is added to the system as reinforcing component filler, forming a uniform network and stable 3D structure in the mixed solution with PVA through hydrogen bonding and supramolecular interaction. Song prepared a cellulose-PVA hydrogel material. They found that after adding cellulose, the mechanical strength of the composite material was significantly enhanced, and the structural stability of the material was improved [34].

Foam molding technology has developed quickly in the past few decades. As an anionic surfactant, SDS has been widely used to foam cellulosic suspensions [35-37]. Lee successfully prepared porous 3D cellulose foam using 3D printing and foaming technology, with good mechanical properties and interesting structure [38]. In this research, cellulose/PVA/EG 3D porous foam was physically cross-linked. Then the PEG and SDS were washed away in the subsequent washing process (Figure 4) and

initially utilized SDS as a foaming agent and surfactant to prepare foam material. Compared with CPS and CPSG, SDS is the key to porous forming. Foam is a complex gas/liquid dispersion system. In the effect of high shear force, massive bubbles are generated and accumulated in a trace amount of surfactant solution to form liquid foam slurry [39]. As shown in Figure 3, those irregular bubbles fix the cellulose and EG particles between the gas and liquid phases [40]. In addition, the liquid foam can be prepared by rearranging SDS molecules at the surface of air bubbles entrapped in a suspension [41]. The hydrophobic area of SDS extends out of the bubble surface, and the hydrophilic area combines with water to form a surfactant layer. The negative charge of cellulose and EG caused electrostatic repulsion with SDS. So, they are repelled between the bubbles to form a water layer containing cellulose and EG. Although it has the same charge as cellulose and EG, they still adsorb to hydrophobic sites to form aggregates as SDS is a strong surfactant [42].

Influence of different factors on adsorption performance

Adsorption is a surface phenomenon in which the solid surface of the adsorbent is bonded by adsorptive molecules (gas/liquid/solid phase). The whole adsorption process is mainly divided into three steps: (1) Film diffusion is also called external diffusion, in which the adsorbate is transported to the external surface of the adsorbent in the space; (2) Intraparticle Diffusion (IPD), means that the adsorbate diffuses from the external surface of the adsorbent into the pores; (3) Surface reaction, means that the adsorbate is adsorbed on the inner surface of the adsorbent [43,44]. In this case, the mass transfer effect needs to be considered. In the adsorption process, the first two steps are mass transfer, and the last step is the reaction step. The adsorption efficiency is determined by the adsorption resistance. Any step of the adsorption resistance in the above steps will have a huge impact on the total adsorption efficiency [45].

At first, transmission resistance is affected by many factors, including the type and structure of the adsorbent. We investigated the adsorption performance of different samples at relatively lower dye concentrations (25 mg/L). As seen in Figure 5A, CPSG has the highest removal rate of dye (96.21%) and adsorption capacity (12.03 mg/g) compared to CP (16.51%, 2.06 mg/g) and CPS (65.02%, 8.13 mg/g). This is mainly due to the porous structure of CPSG, and MB molecules easily diffuse from the external surface to the internal surface. Moreover, EG provides more active sites and significantly improves the adsorption performance.

In addition, the effect of different initial dye concentrations (25 mg/L–250 mg/L) on the adsorption performance was investigated. It can be seen from Figure 5B that as the initial dye concentration increases, the adsorption capacity increases significantly from 12.03 mg/g to 110.81 mg/g, which is possibly caused by concentration polarization. At higher dye concentration, concentration polarization accelerates the diffusion rate of MB molecules on the surface of the adsorbent, and more dye molecules are adsorbed [46].

The pH value is also one of the important factors influencing adsorption performance. The research results show that the removal rate and adsorption capacity of MB increases with the increase of pH value, which is consistent with the relative researches (Figure 5C) [30,46,47]. At low pH, due to protonation, the positive charge on the surface of the material increases, which causes repulsion between cationic dyes and positively composite, resulting in low adsorption efficiency [48].

Moreover, the influence of different temperatures on the adsorption performance was investigated. It can be seen from Figure 5D that as the temperature increases the dye removal rate and adsorption capacity of the adsorbent decrease significantly, indicating that temperature is also an important influencing factor of the adsorption performance. As the temperature increases, the thermal mobility of dye molecules increases, which may accelerate their transport to the surface of the adsorbent. However, at the same time, it may also accelerate the desorption of dye molecules from the surface of the adsorbent [49].

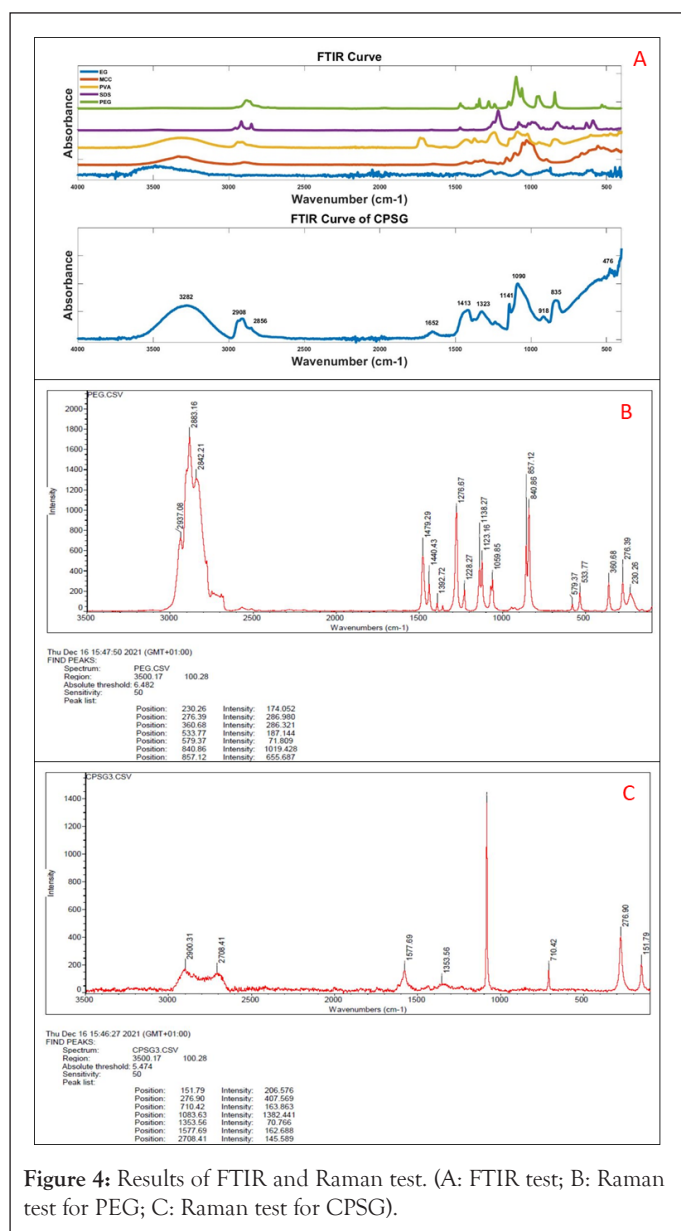


Figure 4: Results of FTIR and Raman test. (A): FTIR test; B): Raman test for PEG; C): Raman test for CPSG.

Adsorption kinetic of adsorbent in MB

There are two possible interactions between adsorbate and adsorbent, namely chemical and physical interaction. Among them, chemical interaction is also called chemical adsorption in that there are chemical or covalent bonds between adsorbate and adsorbent by sharing or transferring electrons. On the other hand, the main force that dominates physical adsorption is van der Waals forces mainly [50].

It is very important to figure out whether an adsorption phenomenon is a chemical or physical adsorption, which can help us understand its adsorption mechanism. Adsorption kinetics reveals the relationship between adsorption efficiency and time and is a good tool to analyze the adsorption rate. This research chooses the three most commonly used kinetic models to study the adsorption rate, as shown in Table 1.

Batch adsorption experiments were performed with different concentrations of dye solutions at 25°C, and the samples were tested every 30 minutes. The adsorption kinetics curves and parameters are shown in Figure 6 and Table 2. It is obvious that the Pseudo-2nd order is more suitable than the Pseudo-1st order. It reveals that the adsorption process depends on the number of active sites [51].

However, some research has reported that the kinetic data near equilibrium may have serious deviations if a Pseudo-2nd order kinetic model is applied [52]. Therefore, other models are needed for further study on the adsorption rate.

The IPD model is used to determine the rate-limiting steps of the entire adsorption process. As shown in Figure 6 and Table 2, $k_{i-1stage} > k_{i-2stage} > k_{i-3stage}$ indicates changes in diffusion rate, revealing that the adsorption process mainly follows three steps: (1) The first stage is the diffusion of MB molecules from the body to the external surface of the adsorbent; (2) Then, MB molecules diffuse through the pores and diffuse into the internal surface; (3) The last stage is near equilibrium stage. In this stage, the balance of adsorption and desorption is reached.

Adsorption isotherm of adsorbent in MB

The adsorption isotherm is to study the relationship between the concentration of adsorbate in the liquid phase and the adsorbent at a specific temperature at equilibrium. Modeling the equilibrium adsorption data can help us study the adsorption mechanism, the interaction between the adsorbate and the adsorbent, the maximum adsorption capacity, and so on [53]. In this study, several models were selected to analyze the adsorption mechanism (Table 3).

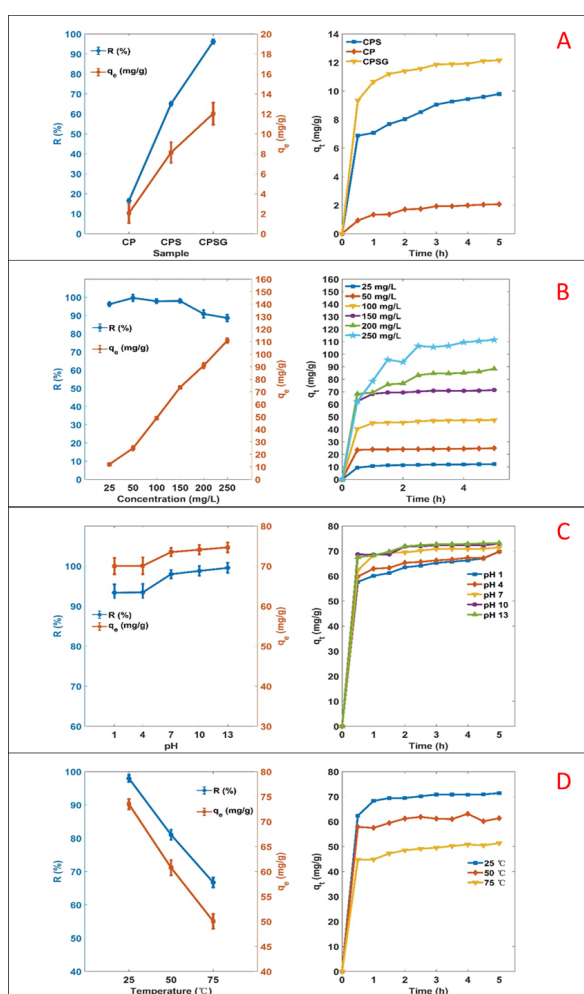


Figure 5: (A) The influence of CP, CPS, and CPSG on adsorption, (B) The effect of different initial concentrations of dyes on adsorption, (C) The influence of different pH values on adsorption, (D) The effect of temperature on adsorption.

Table 1: Adsorption kinetic model used in this study.

Kinetic models	Linearized form
Pseudo-1 st order	$\ln(q_e - q_t) = \ln q_e - k_1 t$
Pseudo-2 nd order	$\frac{t}{q_t} = \frac{1}{k_2 q_e^2} + \frac{t}{q_e}$
IPD model	$q_t = k_1 t^{0.5} + C$

Note: Where q_e (mg/g) and q_t (mg/g) are the adsorption capacity at equilibrium and time, respectively. q_t (h) is the time, k_1 , k_2 and C are Pseudo-1st order, Pseudo-2nd order, and IPD rate constant, respectively. C is a constant related to the thickness of the boundary layer.

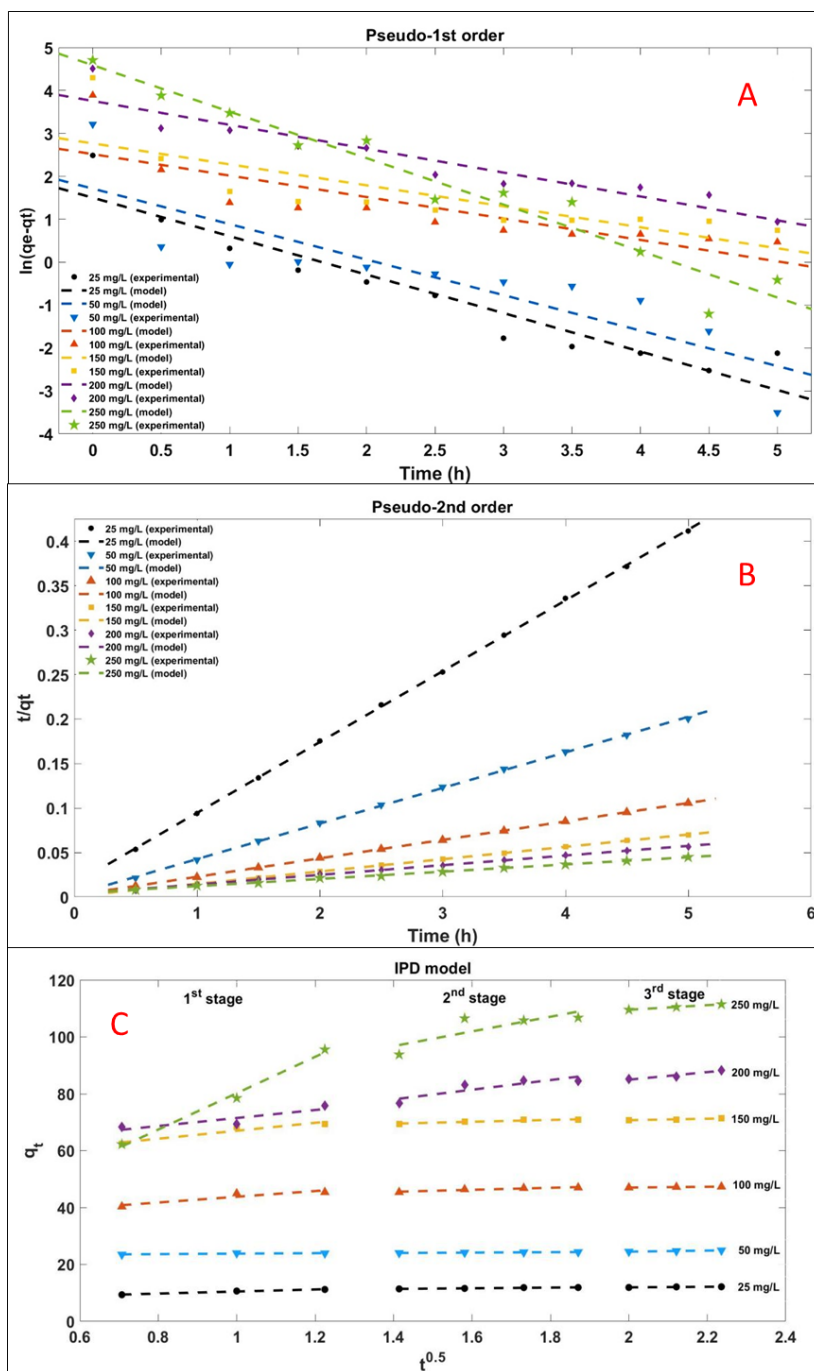


Figure 6: Adsorption kinetic models. A: Pseudo-1st order; B: Pseudo-2nd order; C: IPD model.

Table 2: Parameters of adsorption kinetic.

Models	Parameters	25 mg/L	50 mg/L	100 mg/L	150 mg/L	200 mg/L	250 mg/L
Pseudo-1 st order	q _{e,exp} (mg/L)	12.03	24.91	48.94	73.49	90.9	110.81
	q _{e,cal} (mg/L)	4.49	5.55	12.4	15.92	42.84	98.5
	k ₁ (min ⁻¹)	-0.8963	-0.8271	-0.4998	-0.4887	-0.5565	-1.083
	R ²	0.902	0.741	0.688	0.629	0.888	0.944
Pseudo-2 nd order	q _{e,exp} (mg/L)	12.03	24.91	48.94	73.49	90.9	110.81
	q _{e,cal} (mg/L)	12.56	25.06	48.19	72.2	92.17	123.03
	k ² (min ⁻¹)	0.424	0.613	0.221	0.2014	0.037	0.0161
	R ²	0.999	0.999	0.999	0.999	0.998	0.998
IPD 1 Stage	k _i	1.86	3.64	10.07	13.97	17	63.95
	C	20.77	6.84	33.72	53.03	54.24	16.26
	R ²	0.998	0.976	0.872	0.911	0.768	0.992
IPD 2 Stage	k _i	0.85	1.16	3.53	3.26	14.08	25.81
	C	22.95	9.76	40.59	64.94	57.4	60.64
	R ²	0.715	0.939	0.915	0.912	0.797	0.649
IPD 3 Stage	k _i	0.72	1.02	1.36	2.61	13.33	8.17
	C	23.01	9.89	44.31	65.49	58.29	93.19
	R ²	0.986	0.882	0.984	0.878	0.941	0.999

Table 3: Adsorption isotherm model used in this study.

Isotherm models	Linearized form
Langmuir	$\frac{C_e}{q_e} = \frac{1}{bq_m} + \frac{C_e}{q_m}$
Freundlich	$\ln q_e = \ln k_f - \frac{1}{n} \ln C_e$
Temkin	$q_e = B_1 \ln A + B_1 \ln C_e$

Note: Where q_m is the maximum adsorption capacity, C_e (mg/L) is the equilibrium concentration of dye solution, b is the Langmuir constant, k_f and n are Freundlich constants, B_1 (Jmol⁻¹) and A (L/mg) are the Temkin constant and the equilibrium bond constant.

It can be seen from Figure 7 and Table 4 that the Freundlich model (R²=0.954, 0.991, 0.979) is more suitable than Langmuir (R²=0.983, 0.863, 0.771) and Temkin model (R²=0.935, 0.871, 0.919) for describing the adsorption of MB molecules on cellulose/PVA/EG porous materials. It reveals the multilayer adsorption of MB on heterogeneous surfaces. Multilayer adsorption is due to mutual attraction between molecules, and additional molecules are superimposed on the first adsorption layer to form multilayer adsorption. In addition, n represents the adsorption strength of the adsorbent. When $n > 1$, it indicates that the adsorption behavior is favorable [47]. At the same time, porous adsorbent has greater adsorption strength at 25°C as the lowest temperature in the test, indicating that high temperature is unfavorable for the adsorption behavior.

Thermodynamic of adsorption

Adsorption thermodynamic is used to survey the trend, degree, and driving force of the adsorption process and plays an important role in explaining the characteristics, laws, and mechanism of adsorption. The changes of parameters of thermodynamic of the adsorption process are generally calculated by equations of Gibbs equation and Vant’ Hoffs equation 3, 4 and 5 [54]:

$$\Delta G = -RT \ln K_c \dots\dots\dots(3)$$

$$K_c = \frac{q_e}{c_e} \dots\dots\dots(4)$$

$$\ln K_c = \frac{\Delta S}{R} - \frac{\Delta H}{T} \dots\dots\dots(5)$$

Where ΔG (kJ/mol) is Gibbs free energy, R and T are gas constant (8.314 J/mol/K) and absolute temperature (K), K_c (L/mol) is the equilibrium constant of adsorption, ΔS and ΔH are entropy and enthalpy, respectively.

As shown in Table 5, the free energy ΔG is negative, indicating that the porous material adsorbs MB as a spontaneous process. As the temperature increases, the absolute value of ΔG decreases, indicating that the spontaneous tendency of adsorption decreases, which is not conducive to adsorption? The negative value of the adsorption enthalpy ΔH reveals that the adsorption process is an exothermic reaction. The negative value of the adsorption entropy ΔS indicates that the adsorption reduces the degree of freedom of the adsorbate molecules.

Reusability of the adsorbent

For industrial applications, the regeneration and recycling of adsorbents are very important. In this study, the adsorbent after adsorption was immersed in an ethanol solution to regenerate it. The experimental result shows that after five cycles, the MB dye removal rate of the composite material drops from 97.98%

to 71.93%, possibly for a combination of chemistry and physics adsorption of cellulose/PVA/EG foam. As is known to all, chemical adsorption is irreversible, but physical adsorption is reversible. Therefore, the adsorption process was mainly led by physical adsorption in the subsequent cycle. To sum up, the removal rate of adsorbents after regeneration remains high, which is appropriate for the treatment of MB waste water (Figure 8).

Adsorption mechanism of cellulose/PVA/EG foam in MB

The adsorption mechanism of the adsorbate on the adsorbent

is affected by many factors, such as the size and structure of the adsorbent. Based on the above experimental results, the adsorption mechanism scheme is listed in Figure 9. According to analyzing adsorption kinetics and isotherm, the adsorption process is mainly physical adsorption affected by the number of active sites and adsorbent structure. So, the possible interactions that determine the effect of MB adsorption are electrostatic adsorption, hydrogen bonding, and van der Waals force.

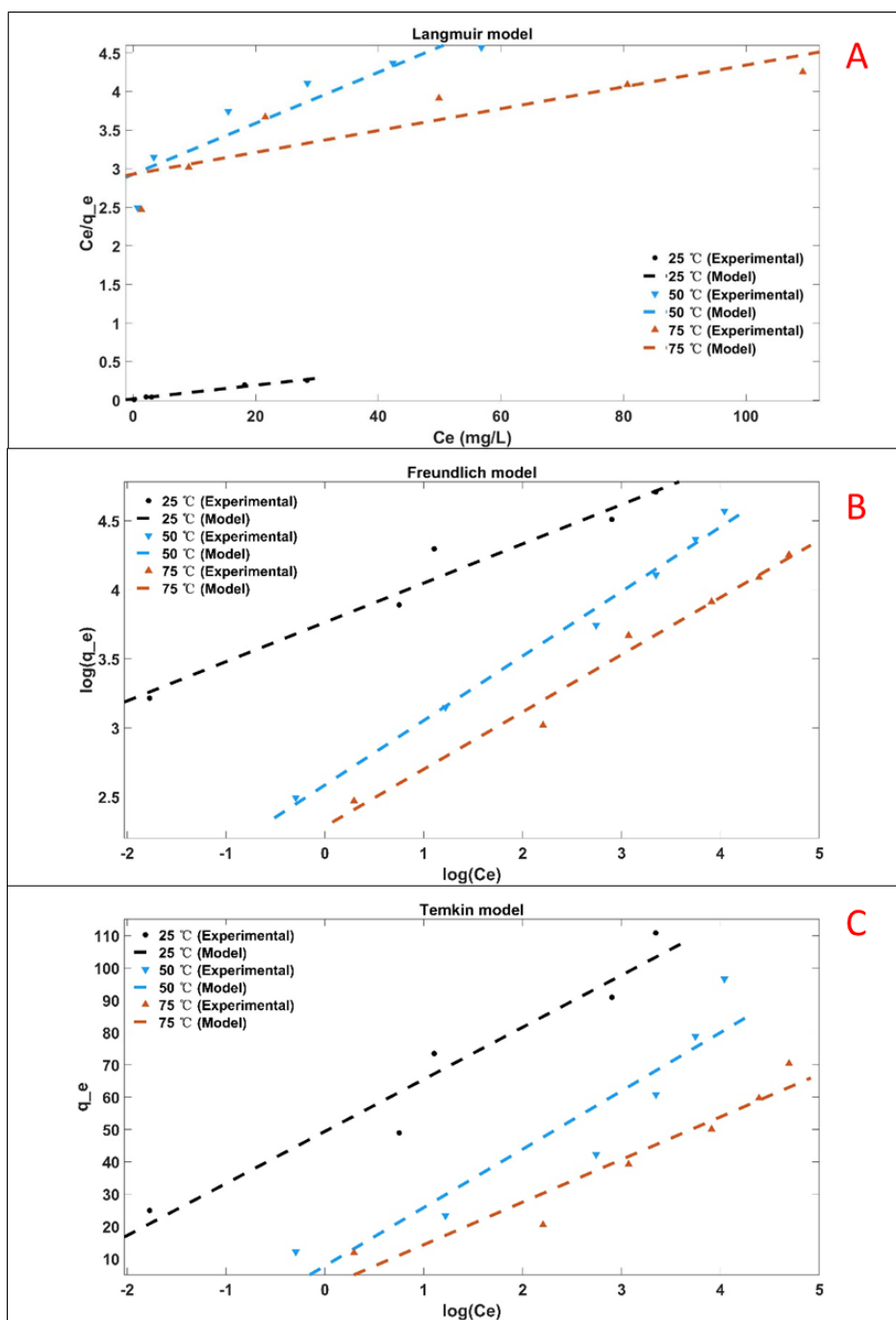


Figure 7: Adsorption isotherm models. (A) Langmuir model; (B) Freundlich model; (C) Temkin model.

Table 4: Key parameters of adsorption isotherm model.

Parameters	Langmuir			Freundlich			Temkin		
	q_m (mg/g)	b (L/mg)	R^2	k_f (L/mg)	n	R^2	B_1 (Jmol ⁻¹)	A (L/mg)	R^2
25°C	112.38	0.5161	0.983	43.1121	3.516	0.954	16.12	21.4108	0.935
50°C	30.3	0.0113	0.863	13.2766	2.1404	0.991	18.06	1.5371	0.871
75°C	70.72	0.0048	0.771	9.8355	2.4114	0.979	13.19	1.0879	0.919

Table 5: Parameters of the thermodynamic model.

Parameters	ΔG (kJ/mol)	ΔH (kJ/mol)	ΔS (kJ/mol/K)
25°C	-7.9121	-55.7537	-0.1622
50°C	-2.0405		
75°C	-0.0663		

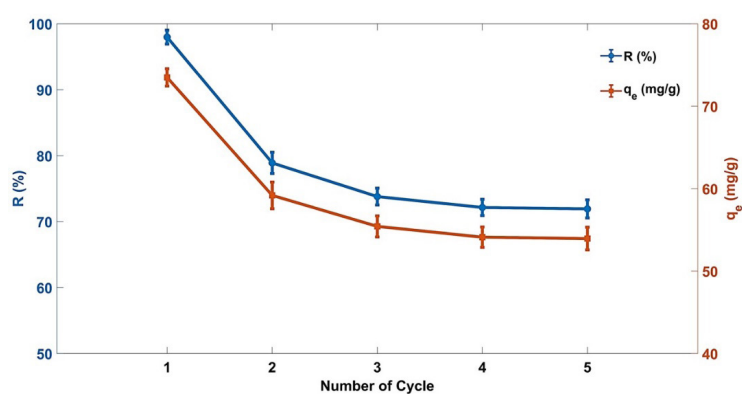


Figure 8: Reusability of porous foam composites in MB adsorption.

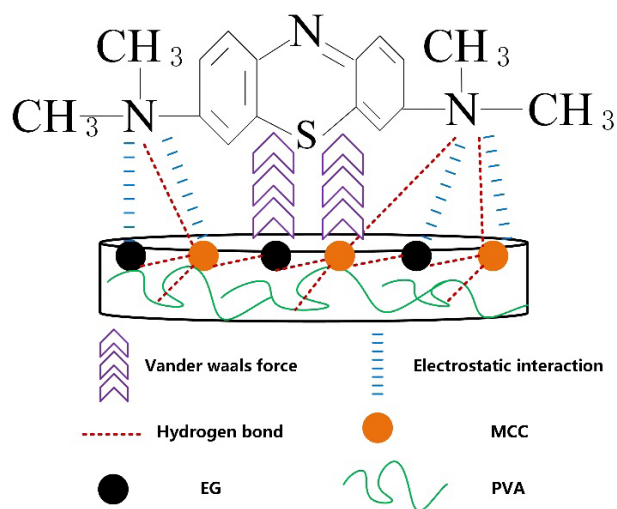


Figure 9: Possible interaction mechanism between cellulose-based porous foam material and MB molecule.

Table 6: Adsorption performance of different adsorbents on MB molecules.

Adsorbent	Concentration of MB	Removal percentage (%)	qe (mg/g)	Reference
Cellulose based porous foam composites	250 mg/L	90.9	110.8	This research
Maghemite/alginate/functionalized multiwalled carbon nanotubes	230 mg/L	-	905.5	[55]
CMC/GOCOOH composite microbeads	250 mg/L	72.09	180.32	[56]
CMC-Alg/GO hydrogel beads	15 mg/L	96.2	78.5	[57]
Salecan-g-PAI	500 mg/L	22.1	107.1	[58]
Magnetic chitosan/clay beads	100 mg/L	-	82	[59]
Activated carbon/cellulose biocomposite films	100 mg/L	-	103.66	[60]

Comparison to other adsorbents of adsorption performance in MB

As shown in Table 6, the adsorbent has significant advantages. The main components of the materials are cellulose, PVA, and EG. These materials are low-cost, renewable, easy to recycle, and degraded. Although the materials developed by Boukhalfa N, and Eltaweil AS have high adsorption capacity [55-56], the cost of their adsorption materials, such as carbon nanotubes or graphene oxide, is very high.

CONCLUSION

In this study, cellulose/PVA/EG 3D porous foam material was prepared by a simple foaming technique using physical crosslinking, and it was evaluated as a “green” and efficient adsorption material. Results show that cellulose strongly supports the 3D network structure of the material, and SDS effectively promotes the formation of the porous structure. The addition of EG significantly improves the removal efficiency of methylene blue. In the adsorption experiment, the dye concentration, pH, and temperature significantly affect the adsorption result of the material. The adsorption capacity is directly proportional to dye concentration and pH, while the adsorption capacity is inversely proportional to temperature. The adsorption process follows the pseudo-2nd order kinetics and Freundlich isotherm model. Thermodynamic studies have shown that the adsorption process is a spontaneous and exothermic reaction. In addition, after five cycles of adsorption, the repeatability study found that the dye removal rate remained high, although the adsorption capacity of the material decreased slightly. Therefore, the prepared cellulose/PVA/EG 3D porous foam material is a stable, environmentally friendly, efficient, and reusable adsorbent for methylene blue removal.

ACKNOWLEDGMENT

The work was supported by the project ‘Advanced structures for thermal insulation in extreme conditions’ (Reg. No. 21-32510

M) granted by the Czech Science Foundation (GACR) and was supported by the research project of Student Grant Competition of Technical University of Liberec no. 2022-6069 and no. 2020-6031 granted by Ministry of Education Youth and Sports of Czech Republic.

DECLARATION OF COMPETING INTEREST

We have no known competing financial interests or personal relationships that could have appeared to influence the work reported in this paper.

REFERENCES

- Yang L, Zhan Y, Gong Y, Ren E, Lan J, Guo R. Development of eco-friendly CO₂-responsive cellulose nanofibril aerogels as “green” adsorbents for anionic dyes removal. *J Hazard Mater.* 2021;405:124194.
- Radwan EK, El-Naggar ME, Abdel-Karim A, Wassel AR. Multifunctional 3D cationic starch/nanofibrillated cellulose/silver nanoparticles nanocomposite cryogel: Synthesis, adsorption, and antibacterial characteristics. *Int J Biol Macromol.* 2021;189:420-431.
- Li J, Li H, Yuan Z, Fang J, Chang L, Zhang H. Role of sulfonation in lignin-based material for adsorption removal of cationic dyes. *Int J Biol Macromol.* 2019;135:1171-1181.
- Bhatti HN, Safa Y, Yakout SM, Shair OH, Iqbal M, Nazir A. Efficient removal of dyes using carboxymethyl cellulose/alginate/polyvinyl alcohol/rice husk composite: Adsorption/desorption, kinetics and recycling studies. *Int J Biol Macromol.* 2020;150:861-870.
- Oz M, Lorke DE, Hasan M, Petroianu GA. Cellular and molecular actions of Methylene Blue in the nervous system. *Med Res Rev.* 2011;31(1):93-117.
- Jiang L, Zhang Y, Zhou M, Liang L, Li K. Oxidation of Rhodamine B by persulfate activated with porous carbon aerogel through a non-radical mechanism. *J Hazard Mater.* 2018;358:53-61.
- Ge X, Wu Z, Cravotto G, Manzoli M, Cintas P, Wu Z. Cork wastewater purification in a cooperative flocculation/adsorption process with microwave-regenerated activated carbon. *J Hazard Mater.* 2018;360:412-419.

8. Liu P, Zhu C, Mathew AP. Mechanically robust high flux graphene oxide-nanocellulose membranes for dye removal from water. *J Hazard Mater.* 2019;371:484-493.
9. Usmani Z, Sharma M, Awasthi AK, Sivakumar N, Lukk T, Pecoraro L, Bioprocessing of waste biomass for sustainable product development and minimizing environmental impact. *Bioresour Technol.* 2021;322:124548.
10. Azha SF, Shahadat M, Ismail S. Acrylic polymer emulsion supported bentonite clay coating for the analysis of industrial dye. *Dyes Pigm.* 2017;145:550-560.
11. Bhatti HN, Hayat J, Iqbal M, Noreen S, Nawaz S. Biocomposite application for the phosphate ions removal in aqueous medium. *J Mater Res Technol.* 2018;7(3):300-307.
12. Hasanzadeh M, Simchi A, Far HS. Nanoporous composites of activated carbon-metal organic frameworks for organic dye adsorption: Synthesis, adsorption mechanism and kinetics studies. *J Ind Eng Chem.* 2020;81:405-414.
13. Youcef LD, Belaroui LS, López-Galindo A. Adsorption of a cationic methylene blue dye on an Algerian palygorskite. *Appl Clay Sci.* 2019;179:105145.
14. Huang Z, Li Y, Chen W, Shi J, Zhang N, Wang X, Modified bentonite adsorption of organic pollutants of dye wastewater. *Mater Chem Phys.* 2017;202:266-276.
15. Al-Ghouti MA, Al-Absi RS. Mechanistic understanding of the adsorption and thermodynamic aspects of cationic methylene blue dye onto cellulosic olive stones biomass from wastewater. *Sci Rep.* 2020;10(1):1-8.
16. Li X, Li Y, Zhang S, Ye Z. Preparation and characterization of new foam adsorbents of poly (vinyl alcohol)/chitosan composites and their removal for dye and heavy metal from aqueous solution. *Chem Eng J.* 2012;183:88-97.
17. Hu Z, Cai L, Liang J, Guo X, Li W, Huang Z. Green synthesis of expanded graphite/layered double hydroxides nanocomposites and their application in adsorption removal of Cr (VI) from aqueous solution. *J Clean Prod.* 2019;209:1216-1227.
18. Verma A, Thakur S, Mamba G, Gupta RK, Thakur P, Thakur VK. Graphite modified sodium alginate hydrogel composite for efficient removal of malachite green dye. *Int J Biol Macromol.* 2020;148:1130-1139.
19. Franco P, Cardea S, Taberner A, de Marco I. Porous aerogels and adsorption of pollutants from water and air: A review. *Molecules.* 2021;26(15):4440.
20. Tang S, Xia D, Yao Y, Chen T, Sun J, Yin Y, Dye adsorption by self-recoverable, adjustable amphiphilic graphene aerogel. *J Colloid Interface Sci.* 2019;554:682-691.
21. Wang S, Ning H, Hu N, Huang K, Weng S, Wu X, Preparation and characterization of graphene oxide/silk fibroin hybrid aerogel for dye and heavy metal adsorption. *Compos B Eng.* 2019;163:716-722.
22. Karami D. A review of aerogel applications in adsorption and catalysis. *J Pet Sci Technol.* 2018;8(4):3-15.
23. Asim N, Badiie M, Alghoul MA, Mohammad M, Fudholi A, Akhtaruzzaman M, Biomass and industrial wastes as resource materials for aerogel preparation: Opportunities, challenges, and research directions. *Ind Eng Chem Res.* 2019;58(38):17621-17645.
24. Lu B, Lin Q, Yin Z, Lin F, Chen X, Huang B. Robust and lightweight biofoam based on cellulose nanofibrils for high-efficient methylene blue adsorption. *Cellulose.* 2021;28(1):273-288.
25. Feng C, Ren P, Huo M, Dai Z, Liang D, Jin Y, Facile synthesis of trimethylammonium grafted cellulose foams with high capacity for selective adsorption of anionic dyes from water. *Carbohydr Polym.* 2020;241:116369.
26. Ma H, Zhang XF, Wang Z, Song L, Yao J. Flexible cellulose foams with a high loading of attapulgite nanorods for Cu²⁺ ions removal. *Colloids Surf A Physicochem Eng Asp.* 2021;612:126038.
27. Yan L, Gao Z. Dissolving of cellulose in PEG/NaOH aqueous solution. *Cellulose.* 2008;15(6):789-796.
28. Cernencu AI, Lungu A, Dragusin D, Serafim A, Vasile E, Ionescu C, Design of cellulose-alginate films using PEG/NaOH aqueous solution as co-solvent. *Cellulose.* 2017;24(10):4419-4431.
29. Tan X, Peng Q, Yang K, Yang T, Saskova J, Wiener J, Preparation and Characterization of corn husk nanocellulose coating on electrospun polyamide 6. *Alex Eng J.* 2022;61(6):4529-4540.
30. Wang Y, Zhao L, Hou J, Peng H, Wu J, Liu Z, Kinetic, isotherm, and thermodynamic studies of the adsorption of dyes from aqueous solution by cellulose-based adsorbents. *Water Sci Technol.* 2018;77(11):2699-2708.
31. Sonker AK, Rathore K, Nagarale RK, Verma V. Crosslinking of Polyvinyl Alcohol (PVA) and effect of crosslinker shape (aliphatic and aromatic) thereof. *J Polym Environ.* 2018;26(5):1782-1794.
32. Kalia S, Dufresne A, Cherian BM, Kaith BS, Avérous L, Njuguna J. Cellulose-based bio-and nanocomposites: A review. *Int J Polym Sci.* 2011.
33. Lavoine N, Desloges I, Dufresne A, Bras J. Microfibrillated cellulose—Its barrier properties and applications in cellulosic materials: A review. *Carbohydr Polym.* 2012;90(2):735-764.
34. Song K, Zhu W, Li X, Yu Z. A novel mechanical robust, self-healing and shape memory hydrogel based on PVA reinforced by cellulose nanocrystal. *Mater Lett.* 2020;260:126884.
35. Alimadadi M, Uesaka T. 3D-oriented fiber networks made by foam forming. *Cellulose.* 2016;23(1):661-671.
36. Hou Q, Wang X. The effect of PVA foaming characteristics on foam forming. *Cellulose.* 2017;24(11):4939-4948.
37. Viitala J, Lappalainen T, Järvinen M. Sodium dodecyl sulphate (SDS) residue analysis of foam-formed cellulose-based products. *Nord Pulp Paper Res J.* 2020;35(2):261-271.
38. Lee H, Kim S, Shin S, Hyun J. 3D structure of lightweight, conductive cellulose nanofiber foam. *Carbohydr Polym.* 2021;253:117238.
39. Weaire D, Phelan R. The physics of foam. *J Phys Condens Matter.* 1996;8(47):9519.
40. Hjelt T, Kinnunen K, Lehmonen J, Beletski N, Hellén E, Liljeström V, Intriguing structural and strength behavior in foam forming. *na;* 2011.
41. Liu Y, Kong S, Xiao H, Bai CY, Lu P, Wang SF. Comparative study of ultra-lightweight pulp foams obtained from various fibers and reinforced by MFC. *Carbohydr Polym.* 2018;182:92-97.
42. Tucker IM, Petkov JT, Penfold J, Thomas RK. Interaction of the anionic surfactant SDS with a cellulose thin film and the role of electrolyte and poyelectrolyte. 2 Hydrophilic cellulose. *Langmuir.* 2012;28(27):10223-10229.
43. Ho YS, Ng JC, McKay G. Kinetics of pollutant sorption by biosorbents. *Sep Purif Technol.* 2000;29(2):189-232.

44. Tan KL, Hameed BH. Insight into the adsorption kinetics models for the removal of contaminants from aqueous solutions. *J Taiwan Inst Chem Eng.* 2017;74:25-48.
45. Amanullah M, Viswanathan S, Farooq S. Equilibrium, kinetics, and column dynamics of methyl ethyl ketone biodegradation. *Ind Eng Chem Res.* 2000;39(9):3387-3396.
46. Eltaweil AS, Mohamed HA, Abd El-Monaem EM, El-Subruiti GM. Mesoporous magnetic biochar composite for enhanced adsorption of malachite green dye: Characterization, adsorption kinetics, thermodynamics and isotherms. *Adv Powder Technol.* 2020;31(3):1253-1263.
47. Abd-Elhamid AI, Kamoun EA, El-Shanshory AA, Soliman HM, Aly HF. Evaluation of graphene oxide-activated carbon as effective composite adsorbent toward the removal of cationic dyes: Composite preparation, characterization and adsorption parameters. *J Mol Liq.* 2019;279:530-539.
48. Premarathna KS, Rajapaksha AU, Sarkar B, Kwon EE, Bhatnagar A, Ok YS. Biochar-based engineered composites for sorptive decontamination of water: A review. *Chem Eng J.* 2019;372:536-550.
49. Sabarish R, Unnikrishnan G. Polyvinyl alcohol/carboxymethyl cellulose/ZSM-5 zeolite biocomposite membranes for dye adsorption applications. *Carbohydr Polym.* 2018;199:129-140.
50. Dabrowski A. Adsorption-from theory to practice. *Adv Colloid Interface Sci.* 2001;93(1-3):135-224.
51. Wang J, Guo X. Adsorption kinetic models: Physical meanings, applications, and solving methods. *J Hazard Mater.* 2020;390:122156.
52. Simonin JP. On the comparison of pseudo-first order and pseudo-second order rate laws in the modeling of adsorption kinetics. *Chem Eng J.* 2016;300:254-263.
53. Wang J, Guo X. Adsorption isotherm models: Classification, physical meaning, application and solving method. *Chemosphere.* 2020;258:127279.
54. Lakouraj MM, Norouziyan RS, Balo S. Preparation and cationic dye adsorption of novel Fe₃O₄ supermagnetic/thiacalix [4] arene tetrasulfonate self-doped/polyaniline nanocomposite: Kinetics, isotherms, and thermodynamic study. *J Chem Eng Data.* 2015;60(8):2262-2272.
55. Boukhalfa N, Boutahala M, Djebri N, Idris A. Maghemite/alginate/functionalized multiwalled carbon nanotubes beads for methylene blue removal: Adsorption and desorption studies. *J Mol Liq.* 2019;275:431-440.
56. Eltaweil AS, Elgarhy GS, El-Subruiti GM, Omer AM. Carboxymethyl cellulose/carboxylated graphene oxide composite microbeads for efficient adsorption of cationic methylene blue dye. *Int J Biol Macromol.* 2020;154:307-318.
57. Allouss D, Essamlali Y, Amadine O, Chakir A, Zahouily M. Response surface methodology for optimization of methylene blue adsorption onto carboxymethyl cellulose-based hydrogel beads: Adsorption kinetics, isotherm, thermodynamics and reusability studies. *RSC advances.* 2019;9(65):37858-37869.
58. Qi X, Wei W, Su T, Zhang J, Dong W. Fabrication of a new polysaccharide-based adsorbent for water purification. *Carbohydr Polym.* 2018;195:368-377.
59. Somsesta N, Sricharoenchaikul V, Aht-Ong D. Adsorption removal of methylene blue onto activated carbon/cellulose biocomposite films: equilibrium and kinetic studies. *Mater Chem Phys.* 2020;240:122221.
60. Bée A, Obeid L, Mbolantenaina R, Welschbillig M, Talbot D. Magnetic chitosan/clay beads: A magnetic adsorbent for the removal of cationic dye from water. *J Magn Magn Mater.* 2017;421:59-64.